

Received April 4, 2021, accepted April 21, 2021, date of publication April 26, 2021, date of current version May 3, 2021.

Digital Object Identifier 10.1109/ACCESS.2021.3075448

Antenna Delay Calibration of UWB Nodes

SHASHI SHAH¹, KRIT CHAIWONG², LA-OR KOVAVISARUCH¹, (Member, IEEE),
KAMOL KAEMARUNGS¹, (Senior Member, IEEE), AND TANEE DEMEECHAI¹

¹National Electronics and Computer Technology Center, National Science and Technology Development Agency, Pathumthani 12120, Thailand

²Faculty of Engineering and Industrial Technology, Phetchaburi Rajabhat University, Phetchaburi 76000, Thailand

Corresponding author: Tanee Demeechai (tanee.demeechai@nectec.or.th)

This work was supported in part by the National Electronics and Computer Technology Center (NECTEC), and in part by the National Science and Technology Development Agency (NSTDA).

ABSTRACT Impulse-radio ultra-wideband (IR-UWB) networks are gaining wide acceptance in short-to-medium range wireless sensing and positioning applications that require high accuracy. It is achieved generally via signal message exchange between ultra-wideband (UWB) transceiver nodes, where the signal propagating through their analog circuitry suffers transmitting and receiving antenna delays. Such delays, unless measured and properly corrected for, may induce an error in range estimation between UWB nodes and eventually affect the accuracy of real-time location systems (RTLs) based on the IR-UWB. This paper presents a system to measure the antenna delays of UWB nodes. It provides comprehensive mathematical modeling, design, and implementation of the proposed antenna delay measurement system. Experimental evaluation in a line-of-sight (LOS) environment shows its effectiveness for maintaining the accuracy of the range measurement between UWB nodes by taking into consideration the antenna delays measured by the proposed system.

INDEX TERMS Air time occupancy, antenna delay, time-of-flight, two-way ranging, ultra-wideband.

I. INTRODUCTION

In a RTL based on an IR-UWB principle, the location of a UWB node is computed from range-based measures relative to other UWB nodes in its vicinity [1]. A commonly used metric is the time-of-flight (TOF), with nanosecond accuracy [2]. The TOF between two UWB nodes is usually estimated by two-way ranging (TWR) methods [3]–[6], which typically rely on the exchange of UWB signal messages between the two nodes.

The TWR methods available in the literature [3]–[6] provide the basis for other variants of TWR methods [7], where they mainly focus on minimizing the TOF error due to the clock offsets that exist between the UWB nodes due to imperfections of the clock oscillators in physical environments [8], [9]. However, TOF accuracy is also affected by delays introduced while acquiring timestamp information of the transmitting and receiving signals by the UWB nodes. Here, the precise timestamp values of events, when a transmitting signal exits the antenna and a receiving signal enters the antenna, are required and vital for the accuracy of the TOF. However, the propagation of a signal from the point

for which the transmission timestamp is determined to the antenna and from the antenna to the point for which the reception timestamp is determined suffers delays, referred to as transmitting and receiving antenna delays [10]. The timestamp values reported by the UWB nodes without knowing the antenna delay values are usually different from the correct timestamp values. This may lead to an error in the calculated range unless the reported timestamps are corrected by taking into account the UWB nodes' antenna delays. The antenna delay depends on the specific device and is caused mainly by the underlying analog circuitry [10]. Although it is very small and varies slightly from device to device, these variations can affect the accuracy of UWB-based RTLs by tens of centimeters since we are measuring radio signals moving at the speed of light. It may not be favorable for indoor RTL applications with stringent localization accuracy [11].

To obtain more accurate UWB-based RTLs, Decawave Ltd. has recently proposed using an iterative TWR based antenna delay measurement method [10] that determines the aggregate antenna delays of the UWB nodes, which can then be used to correct the computed TOF values. In this method, TWR was performed consecutively between each pair of UWB nodes placed with fixed known distances, where candidate values for the antenna delay are uniformly randomly

The associate editor coordinating the review of this manuscript and approving it for publication was Matti Hämäläinen.

generated and altered at each iteration to find a local optimum that produces the least difference between the actual and measured distances. The authors in [12] proposed a method to measure the antenna delay of a UWB node with the help of two other UWB nodes, whose antenna delays do not need to be known or measured, based on the principle of symmetric double-sided TWR (SDS-TWR) [3], [5]. It requires that the UWB nodes should have the same reply-delay times of packet transmission, which may not be feasible for practical implementation with two separate UWB nodes. Aiming to achieve high accuracy, [13] proposed an antenna delay measurement based on the principle of alternative double-sided TWR (AltDS-TWR) [6]. The two methods introduced in [10] and [13] require measurement of the to-and-fro distances between a pair of UWB nodes by performing two separate sessions of TWR between them. This would result in an additional TWR session for each pair of UWB nodes and a relatively longer antenna delay measurement process.

In this paper, we present a novel antenna delay measurement system that measures the antenna delays of a set of two UWB nodes based on UWB communication between them. During the measurement process, the UWB network is set to comprise three nodes and only one TWR session is performed between a pair of nodes to estimate their aggregate antenna delays. We also evaluate the proposed system by an experiment, considering application environments where long-range LOS conditions are not easily obtained, for example, tracking or navigating people in an indoor office. In the experiment, each UWB node is based on Decawave's DW1000 UWB transceiver [14], compliant with the IEEE 802.15.4-2011 UWB standard [5]. Note that Decawave's products have been commercially available for a long time. They are widely used in academia [7], [15] and industry [16], since they provide rich product documentation [17] and user-community discussion forums [18]. The experimental results show that antenna delay-calibrated nodes, which use the values of the antenna delay measured by the proposed system, make more accurate range measurements, with the accuracy being within the same order of magnitude as that obtained from Decawave's method [10] with a lesser number of packets over the air. The main features of the proposed system are summarized below:

- no requirement for prior knowledge of the antenna delays of any of the UWB nodes involved in the measurement process,
- no requirement of clock synchronization between the UWB nodes involved in the measurement process,
- limited air time occupancy with a relatively faster measurement process, and
- a single measurement process provides the antenna delays of two UWB nodes.

II. ANTENNA DELAY MEASUREMENT SYSTEM

A. PROPOSED METHOD

Consider a wireless network of three UWB nodes: M, A, and B, placed at fixed known positions ensuring LOS with

each other. Each node employs a UWB signal with nanosecond accuracy for sample-based timestamps as they leave from and arrive at the transceiver. Hence, based on its clock, each node can determine the transmission or reception timestamp value of a transmitted or received packet with nanosecond accuracy. Also, it can align the transmission time of a packet with a pre-specified timestamp value.

Let M and A transmit the first and second packets of a sensing session, called sensing packets. Denote the time difference of reception of the two packets at node $V \in \{M, A, B\}$ by P_V . Then, for any nodes $X \in \{M, A, B\}$ and $Y \in \{M, A, B\}$, it can be shown that [19]

$$P_X - P_Y = (T_{P(A,X)} - T_{P(A,Y)}) - (T_{P(M,X)} - T_{P(M,Y)}), \quad (1)$$

where $T_{P(X,Y)}$ is the TOF from node X to node Y . Now suppose P_X is to be computed as if it was measured by a preferred clock, and the clock of M is selected as the preferred clock. To facilitate the computation, let M transmit another packet, i.e., the third packet of the sensing session. Note that the transmission time difference between the two sensing packets transmitted by M may be pre-specified. Then, the ratio of the clock-speed of M over the clock-speed of X is given by

$$r_X^M = \begin{cases} 1, & \text{if } X = M \\ \frac{t_{Tx(3)}^M - t_{Tx(1)}^M}{t_{Rx(3)}^X - t_{Rx(1)}^X}, & \text{otherwise,} \end{cases} \quad (2)$$

where $t_{Tx(n)}^X$ and $t_{Rx(n)}^X$ denotes respectively the transmission and reception timestamp values read by X for the n^{th} packet. In addition,

$$\begin{aligned} P_M &= t_{Rx(2)}^M - (t_{Tx(1)}^M + d_M^M) \\ &= P_M^{M,U} - d_M^M, \end{aligned} \quad (3)$$

$$\begin{aligned} P_A &= \{(t_{Tx(2)}^A + d_A^A) - t_{Rx(1)}^A\} r_A^M \\ &= \{t_{Tx(2)}^A - t_{Rx(1)}^A\} r_A^M + d_A^A r_A^M \\ &= P_A^{M,U} + d_A^M, \end{aligned} \quad (4)$$

and

$$\begin{aligned} P_B &= \{t_{Rx(2)}^B - t_{Rx(1)}^B\} r_B^M \\ &= P_B^{M,U}, \end{aligned} \quad (5)$$

where d_X^Y is the aggregate antenna delay (the sum of the transmitting and receiving antenna delays) of X as if it was measured with the clock of Y, and $P_X^{Y,U}$ is the antenna delay-uncalibrated time difference of reception of X as if it was measured with the clock of Y.

After the time difference of reception for each node has been computed, the obtained values from all the three relevant nodes can be collected into a computing unit. With the three numerical values obtained from the three nodes, two independent equations based on (1) can be constructed:

$$P_M - P_B = (T_{P(A,M)} - T_{P(A,B)}) - (T_{P(M,M)} - T_{P(M,B)}), \quad (6)$$

and

$$P_A - P_B = (T_{P(A,A)} - T_{P(A,B)}) - (T_{P(M,A)} - T_{P(M,B)}). \quad (7)$$

Since the three nodes are placed at fixed known positions, the range between each of them can be pre-measured with high accuracy, and subsequently, the TOF values in (6) and (7) can also be measured. Then, substituting the corresponding values of the time difference of reception of nodes M, A, and B from (3), (4), and (5), the above two equations can be reordered to express the antenna delays of nodes M and A as

$$d_M^M = P_M^{M,U} - P_B^{M,U} + T_{P(A,B)} - T_{P(M,A)} - T_{P(M,B)} \quad (8)$$

and

$$d_A^M = P_B^{M,U} - P_A^{M,U} - T_{P(A,B)} - T_{P(M,A)} + T_{P(M,B)}, \quad (9)$$

where

$$P_M^{M,U} = t_{Rx(2)}^M - t_{Tx(1)}^M,$$

$$P_A^{M,U} = (t_{Tx(2)}^A - t_{Rx(1)}^A) \left(\frac{t_{Tx(3)}^M - t_{Tx(1)}^M}{t_{Rx(3)}^A - t_{Rx(1)}^A} \right), \text{ and}$$

$$P_B^{M,U} = (t_{Rx(2)}^B - t_{Rx(1)}^B) \left(\frac{t_{Tx(3)}^M - t_{Tx(1)}^M}{t_{Rx(3)}^B - t_{Rx(1)}^B} \right).$$

B. SYSTEM DESIGN AND IMPLEMENTATION

The system is designed to estimate the antenna delays of two UWB nodes, according to (8) and (9), after a single measurement process. It is set to operate as follows. It includes three UWB nodes configured to act as nodes M, A, and B during the sensing sessions. These three nodes are fully wireless, i.e., the transmission and reception of packets to and from the nodes are over the air. They are set to be placed at fixed known positions ensuring LOS and the actual ranges between all of them are pre-measured. The system also includes two complementary entities: another UWB node, designated as a master node, and a computer (PC). The master node is used to request the initiation of a sensing session, receive the necessary information from the other UWB nodes, and log the data to the PC via a serial UART.

The antenna delay measurement process follows the following sequence.

- *Step 1:* The PC requests the start of the process to the master node.
- *Step 2:* The master node sends an initiation request for a sensing session, where it assigns M to transmit the first and third sensing packets; A to transmit the second sensing packet; and B to listen to the three sensing packets.
- *Step 3:* Node M determines the transmission timestamps for the first and third sensing packets based on its current timestamp value and a properly pre-specified transmission time difference between the two packets.
- *Step 4:* Node M transmits the first sensing packet at the determined time while the other nodes are in receiver mode.
- *Step 5:* Upon completion of transmission and reception, all nodes except M retrieve and store the corresponding reception timestamps. Then A prepares for the transmission of the second sensing packet, while the other nodes enter the receiver mode.

- *Step 6:* Node A transmits the second sensing packet while the other nodes are in receiver mode.
- *Step 7:* Upon completion of transmission and reception, A retrieves and stores the corresponding transmission timestamp, while the other nodes retrieve and store the corresponding reception timestamps. Then M computes its sensing information, transmission/reception timestamp difference values about the first sensing packet respecting the second and third sensing packets, i.e., $t_{Rx(2)}^M - t_{Tx(1)}^M$ and $t_{Tx(3)}^M - t_{Tx(1)}^M$, and prepares for the transmission of the third packet that will carry its sensing information, while the other nodes enter the receiver mode.
- *Step 8:* Node M transmits the third sensing packet at the determined time while the other nodes are in receiver mode.
- *Step 9:* Upon completion of transmission and reception, all nodes except M retrieve and store the corresponding reception timestamps. Node A also retrieves and stores the sensing information of M from the received third sensing packet.
- *Step 10:* Nodes A and B compute their sensing information, i.e., A computes $t_{Tx(2)}^A - t_{Rx(1)}^A$ and $t_{Rx(3)}^A - t_{Rx(1)}^A$, and B computes $t_{Rx(2)}^B - t_{Rx(1)}^B$ and $t_{Rx(3)}^B - t_{Rx(1)}^B$.
- *Step 11:* Upon an information request by the master node, nodes A and B send all the sensing information, i.e., A sends the sensing information of itself and that of M, while B sends the sensing information of itself.
- *Step 12:* The PC receives and stores the sensing information of the sensing session, hereinafter referred as session-data, from the master node.
- *Step 13:* The process of *Step 1* to *Step 12* is repeated until 100 sets of session-data have been stored in the PC.
- *Step 14:* The PC computes the antenna delays for each set of session-data using (8) and (9), which gives 100 estimated antenna delays of M and A, and then averages them to obtain the final antenna delay values for M and A.

Each entity in the system is implemented according to the cooperation mentioned above. The UWB nodes are based on Decawave's DW1000 UWB transceiver [14], and their operations are implemented in C programming using Segger Embedded Studio [20] as an integrated development environment. The operation of the PC is implemented using Python programming.

III. NUMERICAL RESULTS

A. AIR TIME OCCUPANCY

In this section, we analyze and compare the air time occupancy of the proposed system in terms of the number of packets required over the air during a sensing session for obtaining the session-data to estimate the antenna delay of a node. According to the measurement process detailed in Section II-B, the proposed system requires setting up three nodes, involving the transmission/reception of five packets

for a sensing session: three sensing packets and two session-data carrying packets. Here, after a single measurement process, the proposed system estimates the antenna delays of two nodes. Thus, the proposed system observes an average of 2.5 packets over the air to measure the antenna delay of a single node.

For the antenna delay measurement method [10] proposed by Decawave Ltd., a set-up of at least three nodes is required to perform to-and-fro TWR sessions between each possible pair of nodes. Assume that N nodes are present in the set-up, where $N \geq 3$, and to-only TWR sessions are performed between each pair of nodes (to minimize the number of packets over the air). Then each of the $\frac{N(N-1)}{2}$ possible pair of nodes incurs the transmission/reception of four packets during a sensing session: three sensing packets and one packet carrying the session-data. Thus, it would observe an average of $\left(4 \times \frac{N(N-1)}{2}\right)/N = 2(N-1)$ packets over the air to measure the antenna delay of a single node. Notably, the air time occupancy for Decawave's method is dependent on the number of nodes involved during the set-up of the measurement process.

To compare the proposed system with Decawave's method [10], assume $N = 3$ in Decawave's method for its maximum air-time efficiency. Thus, it would observe an average of $2(N-1) = 4$ packets over the air to measure the antenna delay of a single node. Hence, we can conclude that the proposed system is approximately 60% more air efficient for a similar configuration set-up. This may result in a faster measurement process when large samples of session-data are required to be collected to estimate the antenna delays of several nodes.

B. EXPERIMENTAL EVALUATION

In this section, we evaluate the proposed system considering a TWR-based RTLS application in an indoor office, e.g., tracking or navigating people in the office. A TWR-based RTLS consists of several anchors placed at fixed positions. To estimate the position of a tag, TWR is used to estimate the TOFs from the tag to a number of nearby anchors. In this regard, to estimate a three-dimensional position, at least four nearby anchors those are not on the same plane are required. Hence, anchor placement plays a very important role in the system design, affecting its cost and performance. An important consideration for anchor placement is to avoid non-line-of-sight (NLOS) conditions between a tag and nearby anchors. This is because such a condition would produce a positive bias on the estimated TOF that can vary dynamically and significantly as the tag moves around. This source of error is contrasted to antenna delay, which produces a rather quasi-static bias. Currently, although there are available NLOS-mitigation techniques [21]–[23] that can be useful to some extent, a TOF estimated from NLOS conditions cannot be remedied to have LOS-equivalent quality. Hence, we assume a rule of anchor placement such that a tag in the coverage area should typically find LOSs to at least three nearby anchors.

This is to ensure that a TOF from NLOS conditions is only infrequently used in the position estimation. Namely, when a tag sees LOSs to a sufficient number of nearby anchors, the position-estimation process with a LOS/NLOS identification technique [21]–[23] can simply ignore the other nearby NLOS anchors to avoid significant performance impairment. Then, based on our current office building, it seems to be difficult to have LOS over a range greater than 12 m. Therefore, based on the assumed rule of anchor placement, we assume that TOFs of range less than 12 m are typically used by the RTLS in our considered application.

Antenna delay calibration relies on a pre-measurement of the antenna delay, which can then be used in operating applications to correct the TWR bias caused by the antenna delay itself. Such bias correction is considered to be useful only when the LOS condition is the case because the NLOS condition adds a variable bias that needs specific techniques [21]–[23] to deal with. In addition, we do not have a ground truth of the antenna delay of any UWB node. Therefore, we evaluate the accuracy of the proposed system by using it to measure antenna delays of four nodes and then comparing the results of TWR [6] between those nodes for three cases: antenna delay-uncalibrated case, where the antenna delays of the nodes are assumed to be poorly guessed; antenna delay-calibrated (Proposed) case, where the antenna delays of the nodes are measured from the proposed system; and antenna delay-calibrated (Decawave) case, where the antenna delays of the nodes are measured using Decawave's method [10]. Each UWB node is based on the DW1000 device as mentioned. In addition, since the antenna delay also varies with temperature [10], the variation of the ambient temperature is kept minimal during the experiment to minimize its effect on the numerical results. Note that antenna delays have been reported to vary by 2.15 mm/Celsius per device for DW1000 devices [10]. Therefore, a measured antenna delay should be recorded with the corresponding temperature of measurement, so that the value may be adjusted with respect to the operating ambient temperature when the RTLS is under operation.

Let $n1$, $n2$, $n3$, and $n4$ be address identifications of the four nodes whose antenna delays are to be measured. We also take a fifth node with address identification $n5$ to complement the measurement process. To determine the antenna delays of $n1$ and $n2$, we assign $n1$ to act as M, $n2$ to act as A, and $n5$ to act as B during the proposed process of measuring antenna delays. Also, for comparison between methods, Decawave's method with $N = 3$ is executed for $n1$, $n2$, and $n5$, and only the results for $n1$ and $n2$ are recorded. To determine the antenna delays of $n3$ and $n4$, we assign $n3$ to act as M, $n4$ to act as A, and $n5$ to act as B during another implementation of the proposed process of measuring antenna delays. Also, for comparison between methods, Decawave's method with $N = 3$ is executed for $n3$, $n4$, and $n5$, and only the results for $n3$ and $n4$ are recorded. The three nodes in each measurement process were placed at ground level in an indoor LOS environment with coordinates (unit: cm): M = (0, 0),

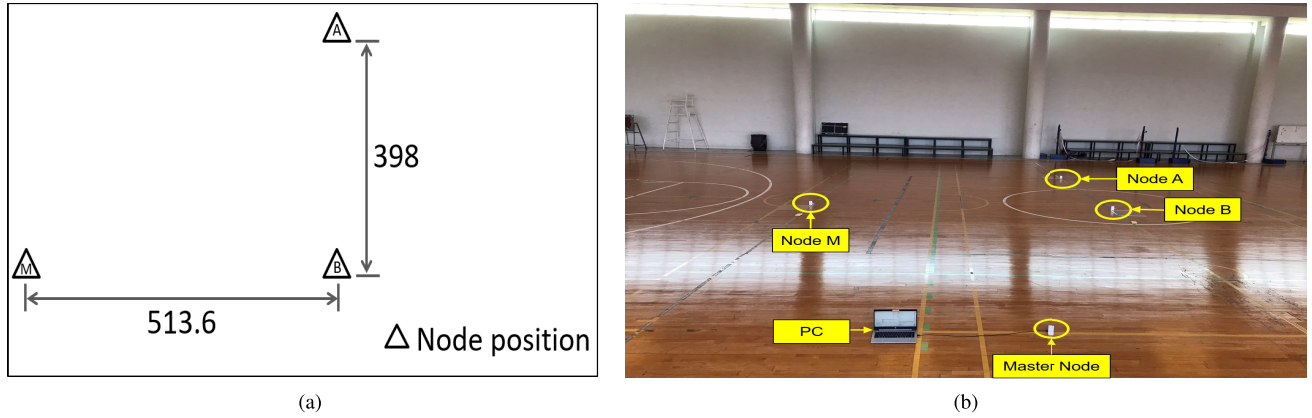


FIGURE 1. (a) Experimental layout (unit: cm; on the floor of an indoor stadium). The positions of the three nodes during the antenna delay measurement process. (b) Measurement environment.

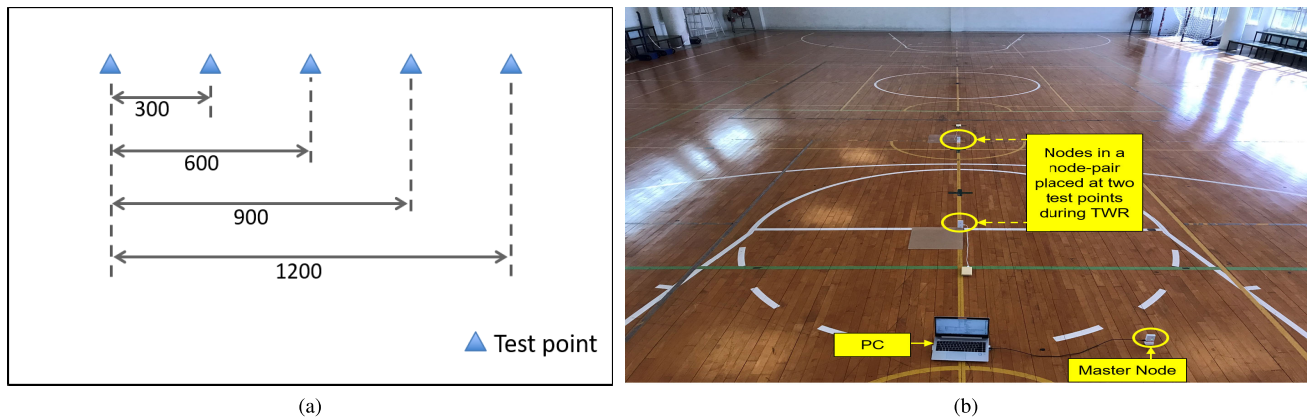


FIGURE 2. (a) Experimental layout (unit: cm; on the floor of an indoor stadium). The test points for positioning of the two nodes in a pair of nodes during the TWR process. (b) Test environment.

$A = (513.6, 398)$, and $B = (513.6, 0)$, as shown in Fig. 1. The three positions were selected keeping in mind that the ranges between the three nodes are to represent typical ranges in the applications discussed above. The measurement results from the proposed method state that the measured antenna delay values (unit: DWT_TIME_UNITS [24]; 15.65 picoseconds ticks) of $n_1 = 69$, $n_2 = 20.2$, $n_3 = 57.4$, and $n_4 = 15.5$. Multiplying these antenna delays by the *speed-of-light* $\times 15.65e-12$, we obtain the corresponding estimated lengths (unit: cm) as $L_{n1} = 32.4$, $L_{n2} = 9.48$, $L_{n3} = 26.94$, and $L_{n4} = 7.28$, where L_X denotes the antenna delay-induced length of node X . Considering a single-sided TWR (SS-TWR) [5] with an ideal clock, an actual range from node X to node Y obtained from the antenna delay-calibrated case, denoted by $R_{(X,Y)}$, can be related to the range obtained from the antenna delay-uncalibrated case, denoted by $R_{(X,Y)}^U$, and the actual antenna delay-induced lengths of X and Y as

$$R_{(X,Y)} = R_{(X,Y)}^U - \left(\frac{L_X + L_Y}{2} \right). \quad (10)$$

Hence (10) can be applied for any related measurement methods as an approximation by substituting the corresponding

values by the estimated values from that measurement method.

For comparison and analysis, each possible pair of the four nodes whose antenna delays were measured, hereinafter referred to as a node-pair, was set to perform AltDS-TWR [6] for the three cases: antenna delay-uncalibrated case, antenna delay-calibrated (Proposed) case, and antenna delay-calibrated (Decawave) case. The two nodes in a node-pair were placed at two test points ensuring LOS for each actual range (unit: cm) from {300, 600, 900, 1200} as shown in Fig. 2. For each case, 100-sample values of the range were obtained for each node-pair placed at the actual ranges, and then the values of the mean and root-mean-square-error (RMSE) were computed for analysis.

The 100-sample means of the ranges estimated by AltDS-TWR for the antenna delay-uncalibrated case and the two antenna delay-calibrated cases are given in Table 1. For all the node-pairs, the results show significant improvement of both the antenna delay-calibrated cases over the antenna delay-uncalibrated case. From the experimental data, the standard deviation (SD) of the estimated ranges at the actual ranges for all three cases were within 4 cm. Also, note that the

TABLE 1. Comparison of mean estimated ranges from AltDS-TWR for antenna delay-uncalibrated and antenna delay-calibrated node-pairs at the actual ranges.

Node-pair	Range (cm)											
	Antenna delay-uncalibrated				Antenna delay-calibrated (Proposed)				Antenna delay-calibrated (Decawave)			
	300	600	900	1200	300	600	900	1200	300	600	900	1200
$n1, n2$	322.3	625.7	926.7	1227.7	301.3	604.8	905.8	1206.8	300.9	604.3	905.3	1206.3
$n3, n4$	318.7	621.9	923.1	1223.8	301.6	604.8	906	1206.7	302.7	605.9	907	1207.8
$n1, n3$	322.8	625.7	927.7	1228.4	293.1	596.1	898.1	1198.8	294.2	597.1	899.1	1199.8
$n1, n4$	320.7	624.3	925.2	1226.5	300.9	604.4	905.3	1206.7	302	605.5	906.4	1207.8
$n2, n3$	321.4	625	925.8	1227	303.2	606.8	907.6	1208.7	302.7	606.3	907.1	1208.2
$n2, n4$	316.5	620.3	920.9	1221.8	308.2	611.9	912.5	1213.5	307.7	611.5	912	1213

relation between the ranges for all possible node-pairs for the antenna delay-uncalibrated case and the antenna delay-calibrated (Proposed) case may be verified using (10). As an example, consider the range estimated by AltDS-TWR for the node-pair ($n1, n2$) at an actual range of 300 cm in Table 1, provided that the measured lengths due to antenna delays of the two nodes are $L_{n1} = 32.4$ cm and $L_{n2} = 9.48$ cm, and the measured range for the antenna delay-uncalibrated case is $R_{(n1,n2)}^U = 322.3$ cm. Then the range for the antenna delay-calibrated (Proposed) case is given by $R_{(n1,n2)} = R_{(n1,n2)}^U - \left(\frac{L_{n1}+L_{n2}}{2}\right) = 322.3 - \left(\frac{32.4+9.48}{2}\right) \approx 301.3$ cm. Similarly, the ranges of all the node-pairs at each actual range for the antenna delay-calibrated (Proposed) case in Table 1 may be obtained by simply following the above relationship shown in (10).

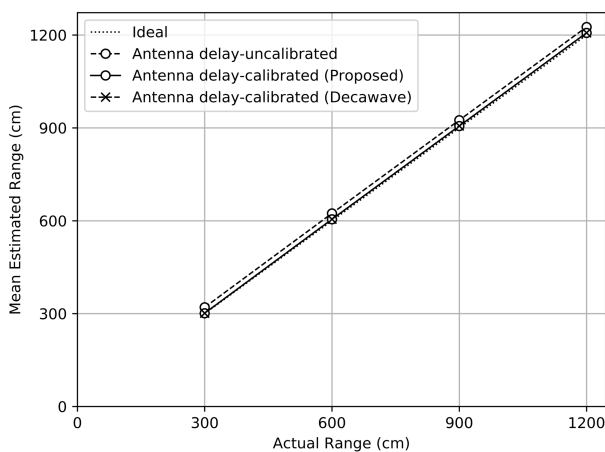


FIGURE 3. Mean of estimated ranges from AltDS-TWR respecting all possible node-pairs vs. actual range.

To compare the estimates of the ranges, Fig. 3 plots the performance of the antenna delay-uncalibrated case and the two antenna delay-calibrated cases at the actual ranges of 300 cm,

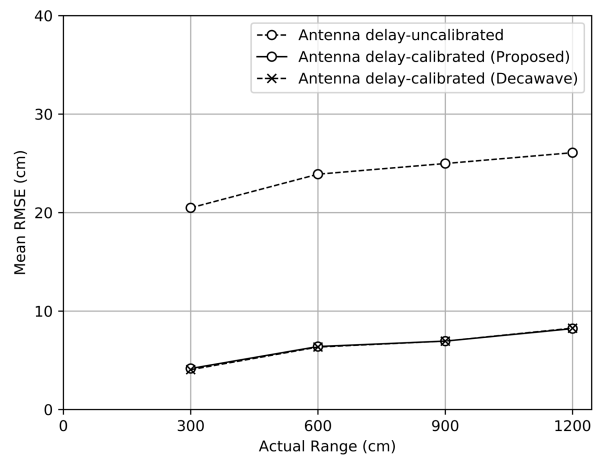


FIGURE 4. Mean of RMSEs from AltDS-TWR respecting all possible node-pairs vs. actual range.

600 cm, 900 cm, and 1200 cm. As seen in Fig. 3, the mean of the estimated ranges respecting all possible node-pairs for the two antenna delay-calibrated cases are close to the actual range (referred to as Ideal). From an analysis of these results, the performances of the antenna delay-calibrated (Proposed) case and antenna delay-calibrated (Decawave) case are similar. In addition, the average improvements over the antenna delay-uncalibrated case in the estimations are approximately 19.02 cm and 18.47 cm.

The values of the RMSE of the ranges estimated using AltDS-TWR for the antenna delay-uncalibrated case and the two antenna delay-calibrated cases of node-pairs are given in Table 2. For all the node-pairs, the RMSEs for the two antenna delay-calibrated cases are significantly improved compared to the antenna delay-uncalibrated case. The RMSEs for the antenna delay-uncalibrated case, antenna delay-calibrated (Proposed) case, and antenna delay-calibrated (Decawave) case are around 24 cm, 7 cm, and 7 cm, respectively. These performance improvements for the two

TABLE 2. Comparison of RMSEs from AltDS-TWR for antenna delay-uncalibrated and antenna delay-calibrated node-pairs at the actual ranges.

Node-pair	RMSE (cm)											
	Antenna delay-uncalibrated				Antenna delay-calibrated (Proposed)				Antenna delay-calibrated (Decawave)			
	300	600	900	1200	300	600	900	1200	300	600	900	1200
$n1, n2$	22.3	25.8	26.8	27.9	2	5.1	6.2	7.6	1.7	4.6	5.8	7.2
$n3, n4$	18.8	22	23.2	24.1	2.3	5.2	6.4	7.6	3.1	6.2	7.4	8.5
$n1, n3$	22.9	25.8	27.8	28.7	7	4.4	2.8	3.8	6	3.4	2.2	3.6
$n1, n4$	20.8	24.3	25.2	26.7	1.8	4.7	5.7	7.3	2.5	5.7	6.7	8.3
$n2, n3$	21.5	25.1	25.9	27.1	3.6	7	7.9	9.2	3.2	6.6	7.4	8.7
$n2, n4$	16.6	20.4	21	22	8.3	12	12.7	13.8	7.8	11.6	12.2	13.3

TABLE 3. Estimated antenna delay bias for antenna delay-uncalibrated and antenna delay-calibrated node-pairs.

Node-pair	Antenna delay bias (cm)		
	Antenna delay-uncalibrated	Antenna delay-calibrated (Proposed)	Antenna delay-calibrated (Decawave)
$n1, n2$	21.17	0.24	-0.23
$n3, n4$	16.59	-0.51	0.57
$n1, n3$	29.15	-0.48	0.55
$n1, n4$	19.3	-0.55	0.54
$n2, n3$	18.47	0.24	-0.25
$n2, n4$	8.62	0.27	-0.21

antenna delay-calibrated cases are noticeable in the plots of Fig. 4. Here, the mean of the RMSEs respecting all possible node-pairs are plotted against the actual range. The results of averaging the RMSEs in Fig. 4 for all the actual ranges of the antenna delay-uncalibrated case, antenna delay-calibrated (Proposed) case, and antenna delay-calibrated (Decawave) case are 23.86 cm, 6.44 cm, and 6.4 cm, respectively. From the results in Table 2 and the plots in Fig. 4, it is clear that the performance improvements of the two antenna delay-calibrated cases over the antenna delay-uncalibrated case are within the same order of magnitude.

A deeper analysis may be required to explain the variation in RMSE in more detail. We have observed from the experimental data that the SD of estimated ranges associated with each RMSE value in Table 2 is small and does not depend considerably on node-pair and calibration case. In other words, for each numerical column of Table 2, the six associated values of the SD are approximately the same: approximately 1.5 cm, 1.73 cm, 2.18 cm, and 3.24 cm for actual ranges of 300 cm, 600 cm, 900 cm, and 1200 cm, respectively. Obviously, the SD increases with the actual range, as a manifestation of receiver noise. In addition, since the SDs are relatively small, we see that the variation of the RMSE in Table 2 is due primarily to a variation in the mean

error, that is, a so-called bias. Here, we consider that the clock-speed offset is well compensated for the AltDS-TWR method. Therefore, the bias defined as the mean estimated range minus the actual range may be approximated by $b_a + b_r$, where b_a is the bias due to antenna delay, and b_r is the power-dependent range bias [25]. Note that both biases depend on analog-circuit variation, i.e., the node-pair. In addition, b_a does not depend on the actual range, and it should be small in the two antenna delay-calibrated cases. On the other hand, b_r does not depend on the calibration case, but it depends on the actual range. Here, we estimate b_a and b_r as follows. Note that (10) implies that b_a for a node-pair (X, Y) in the antenna delay-uncalibrated case may be approximated by $(L_X + L_Y)/2$. Therefore, for each node-pair (X, Y) in the antenna delay-uncalibrated case, b_a is computed by averaging $(L_X + L_Y)/2$ across the two measurement methods. Then b_a for the two antenna delay-calibrated cases and b_r for all actual ranges are estimated by a linear least-squares method. In this way, for each node-pair, the required six bias values are determined from 12 equations, constructed taking the mean estimated range minus the actual range to be $b_a + b_r$ using the data in the corresponding row of Table 1. The results are shown in Tables 3 and 4, where the associated sum of squared errors from the linear least-squares method are

TABLE 4. Estimated range bias for the node-pairs at the actual ranges.

Node-pair	Range bias (cm)			
	300	600	900	1200
$n1, n2$	1.11	4.54	5.54	6.53
$n3, n4$	2.12	5.32	6.49	7.22
$n1, n3$	-6.37	-3.44	-1.44	-0.74
$n1, n4$	1.44	4.98	5.88	7.24
$n2, n3$	2.95	6.55	7.35	8.49
$n2, n4$	7.91	11.68	12.24	13.21

0.005, 0.005, 0.005, 0.0067, 0.005, and 0.0083 respectively for node-pairs $(n1, n2)$, $(n3, n4)$, $(n1, n3)$, $(n1, n4)$, $(n2, n3)$, and $(n2, n4)$. The results in Table 3 confirm that the two calibration methods successfully do their specific duties, i.e., reduce the values of b_a . The results in Table 4 show that the estimated range bias depends considerably on the node-pair, as expected. In addition, the range bias for a node-pair increases with the actual range. This is relevant to the results in [25], which reports that the range bias decreases with received signal power.

From these analyses, we can conclude that the performance of the proposed antenna delay measurement system is comparable to Decawave's method [10], and can effectively handle the bias originating from antenna delays in UWB nodes so that the antenna delay-calibrated UWB nodes provide a more accurate range measurement.

The obtained values of the antenna delays are expected to be applicable when other sources of bias are well managed. Otherwise, the unmanaged bias due to a source may dominate and severely corrupt the TWR results. Experimental results on the use of the obtained delays where the clock-speed offset, which causes a quasi-static bias, is not well managed are presented in Appendix A.

IV. CONCLUSION

This paper has presented a system to measure the antenna delays of nodes in IR-UWB networks. During the measurement process, the system performs a session of TWR and measures the aggregate antenna delays of two UWB nodes. The proposed system requires a lesser number of signaling messages during the process of measuring the antenna delays when compared to Decawave's method, while still achieving a similar level of effectiveness in the accuracy of the measurement of the range. Based on an experiment comparing the ranging in an LOS environment between the UWB nodes that take the antenna delay values measured by the proposed system into consideration, the antenna delay-calibrated nodes provide a more accurate range measurement by effectively handling the range estimation error due to the antenna delays.

APPENDIX A EVALUATION OF THE PROPOSED ANTENNA DELAY MEASUREMENT SYSTEM FOR OTHER TWR METHODS

The obtained antenna delays of the four nodes were also tested with other well-known TWR methods. For each of the three calibration cases, 100 samples of ranges were obtained for each node-pair placed at an actual range (unit:cm) from {300, 600, 900, 1200} as shown in Fig. 2 for two TWR methods: SS-TWR [5] and SDS-TWR [3], [5]. Then, the means and RMSEs were computed for performance analysis. Note that the two TWR methods use the same experimental data, i.e., the timestamp values for computing the ranges, as that of the test for AltDS-TWR in Section III-B. This is possible because the three methods differ only on what and how timestamp values are used in the range estimation [7] and all timestamp values required by the two methods are available in that experimental data. In addition, for both TWR methods, (10) can also be applied as the relation between $R_{(X,Y)}$ and $R_{(X,Y)}^U$.

A. NUMERICAL RESULTS FOR SS-TWR

The 100-sample means and RMSEs of the ranges estimated by SS-TWR for the antenna delay-uncalibrated case and the two antenna delay-calibrated cases of node-pairs are given in Tables 5 and 6 respectively. While we may expect to see a similarity, the results are very much different from those in Tables 1 and 2. We consider that the difference is due solely to the effect of the clock-speed offset, which severely corrupts the estimated ranges. Fortunately, in the experimental data, we recorded the clock-speed offset data based on the `dwt_readcarrierintegrator()` function [24], enabling us to investigate such corruption. In this regard, for each of $100 \times 12 \times 6$ estimated ranges that were used to compute Tables 5 and 6, we obtain a range difference as the SS-TWR estimated range minus the AltDS-TWR estimated range, and a normalized clock-speed offset as an estimation of $(f_{Tx} - f_{Rx})/f_{Rx}$, where f_{Tx} and f_{Rx} are respectively the clock speeds of the transmitting and receiving TWR nodes for the reception of the first sensing packet. The results are then shown as a scatter plot in Fig. 5, from which we see that the range difference is clearly proportional to the normalized clock-speed offset. This confirms that the corruption in the estimated ranges is specifically due to the clock-speed offset. Also, the large variation in the range difference shown in Fig. 5 suggests that the clock-speed offset can be the most dominant source of ranging error in SS-TWR.

Fig. 6 plots the mean of the RMSEs of the ranges estimated by SS-TWR, for the antenna delay-uncalibrated case and the two antenna delay-calibrated cases, respecting all possible node-pairs. From the plots in Fig. 6, we can see performance improvements of the two antenna delay-calibrated cases compared to the antenna delay-uncalibrated case. The results of averaging the RMSEs in Fig. 6 for all the actual ranges of

TABLE 5. Comparison of mean estimated ranges from SS-TWR for antenna delay-uncalibrated and antenna delay-calibrated node-pairs at the actual ranges.

Node-pair	Range (cm)											
	Antenna delay-uncalibrated				Antenna delay-calibrated (Proposed)				Antenna delay-calibrated (Decawave)			
	300	600	900	1200	300	600	900	1200	300	600	900	1200
$n1, n2$	338.5	672.8	887.9	1141.4	317.5	651.8	867	1120.5	317.1	651.4	866.5	1120
$n3, n4$	335.3	639.3	940.7	1241.7	318.1	622.2	923.6	1224.6	319.2	623.2	924.6	1225.6
$n1, n3$	400	693.8	989.6	1285.5	370.3	664.1	959.9	1255.8	371.4	665.2	960.9	1256.9
$n1, n4$	323.2	628.2	929.6	1232.1	303.4	608.3	909.8	1212.3	304.5	609.4	910.9	1213.4
$n2, n3$	337.7	633.8	928.6	1225.6	319.5	615.6	910.4	1207.4	319	615.1	909.9	1206.9
$n2, n4$	287.3	586.5	884.4	1183.6	278.9	578.1	876.1	1175.2	278.4	577.6	875.6	1174.8

TABLE 6. Comparison of RMSEs from SS-TWR for antenna delay-uncalibrated and antenna delay-calibrated node-pairs at the actual ranges.

Node-pair	RMSE (cm)											
	Antenna delay-uncalibrated				Antenna delay-calibrated (Proposed)				Antenna delay-calibrated (Decawave)			
	300	600	900	1200	300	600	900	1200	300	600	900	1200
$n1, n2$	38.5	72.8	12.9	58.7	17.6	51.9	33.4	79.6	17.2	51.4	33.8	80.1
$n3, n4$	35.3	39.4	40.8	41.9	18.2	22.3	23.7	25	19.3	23.4	24.8	26
$n1, n3$	100	93.8	89.6	85.6	70	64.2	59.9	56	71.4	65.2	61	57
$n1, n4$	23.3	28.2	29.7	32.3	3.8	8.5	10.1	12.8	4.8	9.6	11.1	13.8
$n2, n3$	37.8	33.9	28.7	25.9	19.6	15.8	10.6	8.2	19.1	15.3	10.2	7.7
$n2, n4$	12.8	13.6	15.7	16.7	21.2	22	24.1	25	21.6	22.4	24.5	25.4

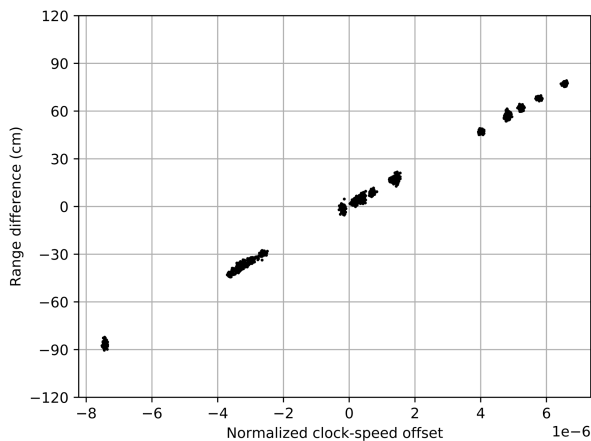


FIGURE 5. Scatter plot of range difference between SS-TWR and AltDS-TWR methods vs. normalized clock-speed offset.

the antenna delay-uncalibrated case, antenna delay-calibrated (Proposed) case, and antenna delay-calibrated (Decawave) case are 42 cm, 29.31 cm, and 29.84 cm, respectively. This shows that although the range results in SS-TWR are severely corrupted by the clock-speed offset, an antenna delay calibration still leads to performance improvements on average.

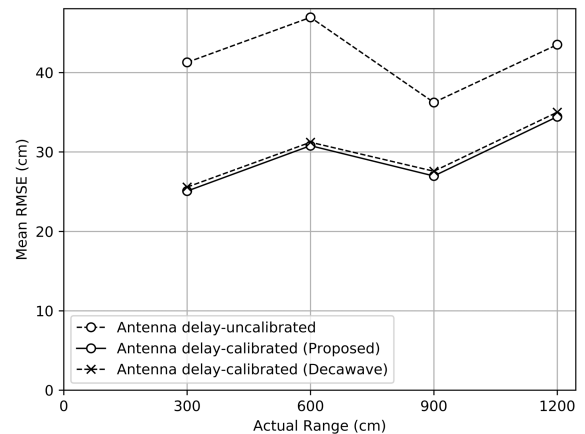


FIGURE 6. Mean of RMSEs from SS-TWR respecting all possible node-pairs vs. actual range.

B. NUMERICAL RESULTS FOR SDS-TWR

The 100-sample means and RMSEs of the ranges estimated by SDS-TWR for the antenna delay-uncalibrated case and the two antenna delay-calibrated cases of node-pairs are given in Tables 7 and 8 respectively. The results are different from those in Tables 1 and 2, and such differences can be

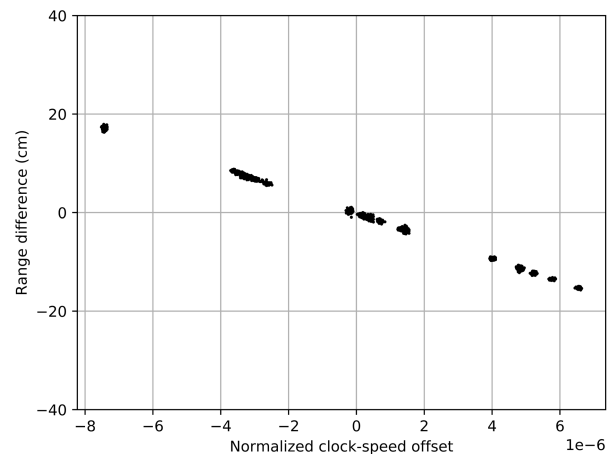
TABLE 7. Comparison of mean estimated ranges from SDS-TWR for antenna delay-uncalibrated and antenna delay-calibrated node-pairs at the actual ranges.

Node-pair	Range (cm)											
	Antenna delay-uncalibrated				Antenna delay-calibrated (Proposed)				Antenna delay-calibrated (Decawave)			
	300	600	900	1200	300	600	900	1200	300	600	900	1200
$n1, n2$	319.1	616.4	934.4	1244.8	298.1	595.4	913.5	1223.9	297.7	595	913	1223.4
$n3, n4$	315.5	618.5	919.6	1220.3	298.3	601.4	902.5	1203.2	299.4	602.4	903.6	1204.2
$n1, n3$	307.5	612.2	915.5	1217.1	277.8	582.6	885.8	1187.5	278.9	583.6	886.9	1188.5
$n1, n4$	320.2	623.5	924.3	1225.4	300.4	603.6	904.4	1205.6	301.5	604.7	905.5	1206.6
$n2, n3$	318.2	623.3	925.3	1227.2	300	605.1	907	1209	299.5	604.6	906.5	1208.5
$n2, n4$	322.3	627	928.1	1229.4	314	618.7	919.7	1221	313.5	618.2	919.3	1220.6

TABLE 8. Comparison of RMSEs from SDS-TWR for antenna delay-uncalibrated and antenna delay-calibrated node-pairs at the actual ranges.

Node-pair	RMSE (cm)											
	Antenna delay-uncalibrated				Antenna delay-calibrated (Proposed)				Antenna delay-calibrated (Decawave)			
	300	600	900	1200	300	600	900	1200	300	600	900	1200
$n1, n2$	19.1	16.5	34.5	44.9	2.3	4.9	13.7	24.1	2.7	5.3	13.2	23.7
$n3, n4$	15.5	18.6	19.8	20.6	2.3	2.4	3.4	4.7	1.7	3.2	4.3	5.5
$n1, n3$	7.6	12.4	15.6	17.5	22.2	17.5	14.3	13	21.2	16.5	13.3	12
$n1, n4$	20.3	23.5	24.4	25.6	1.6	3.9	4.9	6.3	2.1	5	5.9	7.3
$n2, n3$	18.3	23.4	25.3	27.4	1.7	5.4	7.3	9.4	1.8	4.9	6.9	9
$n2, n4$	22.4	27.1	28.2	29.6	14	18.7	19.9	21.2	13.6	18.3	19.4	20.8

considered as due solely to the effect of clock-speed offset, which corrupts the estimated ranges. In this regard, for each of $100 \times 12 \times 6$ estimated ranges that were used to compute Tables 7 and 8, we obtain a range difference as the SDS-TWR estimated range minus the AltDS-TWR estimated range, and a normalized clock-speed offset as an estimation of $(f_{Tx} - f_{Rx})/f_{Rx}$. The results are then shown as a scatter plot in Fig. 7, from which we see that the range difference is clearly proportional to the normalized clock-speed offset. This confirms that the corruption in the estimated ranges is specifically due to the clock-speed offset. The variation in the range difference is relatively small when compared to Fig. 5. This suggests that the ranging error from the clock-speed offset is much less severe in SDS-TWR than in SS-TWR. Moreover, compared to Tables 3 and 4, the range difference results also show that the clock-speed offset is still a dominant source of ranging error. However, SDS-TWR should also have well-compensated the clock-speed offset [6], and in such a case, the range difference should be considerably smaller. The conflicting results are because we have used the timestamp values available in the experimental data to compute the

**FIGURE 7.** Scatter plot of range difference between SDS-TWR and AltDS-TWR methods vs. normalized clock-speed offset.

ranges estimated by SDS-TWR. Such timestamp values were not obtained based on the design principles of SDS-TWR. For an actual implementation of SDS-TWR, we can expect

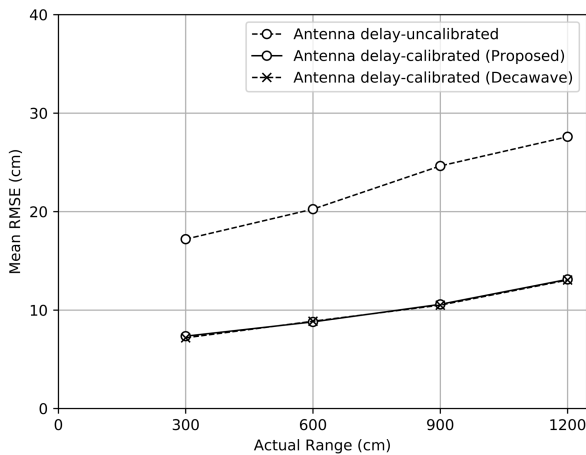


FIGURE 8. Mean of RMSEs from SDS-TWR respecting all possible node-pairs vs. actual range.

results for the ranges and conclusions similar to that of AltDS-TWR.

Fig. 8 plots the mean of the RMSEs of the ranges estimated by SDS-TWR, for the antenna delay-uncalibrated and the two antenna delay-calibrated cases, respecting all possible node-pairs. The plots of Fig. 8 show that the performance of the two antenna delay-calibrated cases is better than the antenna delay-uncalibrated case. Here, the results of averaging the RMSEs in Fig. 8 for all the actual ranges of the antenna delay-uncalibrated case, antenna delay-calibrated (Proposed) case, and antenna delay-calibrated (Decawave) case are 22.42 cm, 9.96 cm, and 9.9 cm, respectively. This shows that although the range results in SDS-TWR are corrupted by the clock-speed offset, antenna delay calibration still yields performance improvements on average.

ACKNOWLEDGMENT

The authors express their sincere gratitude to Mr. Witsarawat Chantaweesomboon and Sirindhorn Science Home (SSH) for assisting and providing space to conduct the experiment.

REFERENCES

- [1] F. Zafari, A. Gkelias, and K. K. Leung, "A survey of indoor localization systems and technologies," *IEEE Commun. Surveys Tuts.*, vol. 21, no. 3, pp. 2568–2599, 3rd Quart., 2019. [Online]. Available: <https://ieeexplore.ieee.org/document/8692423>
- [2] H. Liu, H. Darabi, P. Banerjee, and J. Liu, "Survey of wireless indoor positioning techniques and systems," *IEEE Trans. Syst., Man, Cybern. C, Appl. Rev.*, vol. 37, no. 6, pp. 1067–1080, Nov. 2007. [Online]. Available: <https://ieeexplore.ieee.org/document/4343996>
- [3] R. Hach, "Symmetric double side two way ranging," in *Proc. IEEE Comput. Soc.*, Oct. 2005.
- [4] Y. Jiang and V. C. M. Leung, "An asymmetric double sided two-way ranging for crystal offset," in *Proc. Int. Symp. Signals, Syst. Electron.*, Jul. 2007, pp. 525–528. [Online]. Available: <https://ieeexplore.ieee.org/document/4294528>
- [5] *IEEE Standard for Local and Metropolitan Area Networks—Part 15.4: Low-Rate Wireless Personal Area Networks LR-WPANs*, Standard 802.15.4-2011 Revision IEEE Std 802.15.4-2006, 2011, pp. 1–314. [Online]. Available: <https://ieeexplore.ieee.org/document/6012487>
- [6] D. Neiryneck, E. Luk, and M. McLaughlin, "An alternative double-sided two-way ranging method," in *Proc. 13th Workshop Positioning, Navigat. Commun. (WPNC)*, Oct. 2016, pp. 1–4. <https://ieeexplore.ieee.org/document/7822844>
- [7] C. Lian Sang, M. Adams, T. Hörmann, M. Hesse, M. Pormann, and U. Räckert, "Numerical and experimental evaluation of error estimation for two-way ranging methods," *Sensors*, vol. 19, no. 3, p. 616, Feb. 2019. [Online]. Available: <https://www.mdpi.com/1424-8220/19/3/616>
- [8] S. He and X. Dong, "High-accuracy localization platform using asynchronous time difference of arrival technology," *IEEE Trans. Instrum. Meas.*, vol. 66, no. 7, pp. 1728–1742, Jul. 2017. [Online]. Available: <https://ieeexplore.ieee.org/document/7869397>
- [9] Y.-C. Wu, Q. Chaudhari, and E. Serpedin, "Clock synchronization of wireless sensor networks," *IEEE Signal Process. Mag.*, vol. 28, no. 1, pp. 124–138, Jan. 2011. [Online]. Available: <https://ieeexplore.ieee.org/document/5670639>
- [10] *APS014 Application Note, Antenna Delay Calibration of DW1000-Based Products and Systems*, Decawave, Dublin, Ireland, 2018. [Online]. Available: <https://www.decawave.com/application-notes/>
- [11] A. Basiri, E. S. Lohan, T. Moore, A. Winstanley, P. Peltola, C. Hill, P. Amirian, and P. F. Silva, "Indoor location based services challenges, requirements and usability of current solutions," *Comput. Sci. Rev.*, vol. 24, pp. 1–12, May 2017. [Online]. Available: <http://www.sciencedirect.com/science/article/pii/S1574013716301782>
- [12] K. A. Horvath, G. Ill, and A. Milankovich, "Calibration method of antenna delays for UWB-based localization systems," in *Proc. IEEE 17th Int. Conf. Ubiquitous Wireless Broadband (ICUBW)*, Sep. 2017, pp. 1–5. [Online]. Available: <https://ieeexplore.ieee.org/document/8250969>
- [13] X. Gui, S. Guo, Q. Chen, and L. Han, "A new calibration method of UWB antenna delay based on the ADS-TWR," in *Proc. 37th Chin. Control Conf. (CCC)*, Jul. 2018, pp. 7364–7369. [Online]. Available: <https://ieeexplore.ieee.org/document/8483104>
- [14] *Decawave DWM1001 Datasheet*, Decawave, Dublin, Ireland, 2017. [Online]. Available: https://www.decawave.com/sites/default/files/dwm1001_datasheet.pdf
- [15] A. R. Jimenez Ruiz and F. Seco Granja, "Comparing ubisense, BeSpooon, and DecaWave UWB location systems: Indoor performance analysis," *IEEE Trans. Instrum. Meas.*, vol. 66, no. 8, pp. 2106–2117, Aug. 2017. [Online]. Available: <https://ieeexplore.ieee.org/document/7891540>
- [16] *Decawave Partners*. Accessed: Jan. 6, 2021. [Online]. Available: <https://www.decawave.com/partners/>
- [17] *Decawave Product Documentation*. Accessed: Jan. 6, 2021. [Online]. Available: <https://www.decawave.com/product-documentation/>
- [18] *Decawave Forum*. Accessed: Jan. 6, 2021. [Online]. Available: <https://decaforum.decawave.com/>
- [19] S. Shah and T. Demechai, "Multiple simultaneous ranging in IR-UWB networks," *Sensors*, vol. 19, no. 24, p. 5415, Dec. 2019. [Online]. Available: <https://www.mdpi.com/1424-8220/19/24/5415>
- [20] S. Microcontroller. *Segger Embedded Studio*. Accessed: Oct. 4, 2020. [Online]. Available: <https://www.segger.com/products/development-tools/embedded-studio/>
- [21] S. Marano, W. Gifford, H. Wymeersch, and M. Win, "NLOS identification and mitigation for localization based on UWB experimental data," *IEEE J. Sel. Areas Commun.*, vol. 28, no. 7, pp. 1026–1035, Sep. 2010. [Online]. Available: <https://ieeexplore.ieee.org/document/5555901>
- [22] K. Yu, K. Wen, Y. Li, S. Zhang, and K. Zhang, "A novel NLOS mitigation algorithm for UWB localization in harsh indoor environments," *IEEE Trans. Veh. Technol.*, vol. 68, no. 1, pp. 686–699, Jan. 2019. [Online]. Available: <https://ieeexplore.ieee.org/document/8550815>
- [23] J. Park, S. Nam, H. Choi, Y. Ko, and Y.-B. Ko, "Improving deep learning-based UWB LOS/NLOS identification with transfer learning: An empirical approach," *Electronics*, vol. 9, no. 10, p. 1714, Oct. 2020. [Online]. Available: <https://www.mdpi.com/2079-9292/9/10/1714>
- [24] *DW1000 Device Driver Application Programming Interface (API) Guide*, Decawave, Dublin, Ireland, 2016.
- [25] *APS011 Application Notes, Sources of Error in DW1000 Based Two-Way Ranging (TWR) Schemes*, Decawave, Dublin, Ireland, 2014. [Online]. Available: <https://www.decawave.com/application-notes/>



SHASHI SHAH received the B.Eng. degree in electrical and electronics (communications) from Kathmandu University, Nepal, in 2009, the M.Eng. degree in telecommunications from the Asian Institute of Technology, Thailand, in 2012, and the Ph.D. degree in information science from the Japan Advanced Institute of Science and Technology (JAIST), Japan, in 2018, and in information, computer, and communication technology from the Sirindhorn International Institute of Technology (SIIT), Thammasat University, Thailand, in 2019, under the SIIT-JAIST Doctoral Dual-Degree Program. He is currently a Postdoctoral Researcher with the Location and Automatic Identification (LAI) Laboratory, under the National Electronics and Computer Technology Center (NECTEC), National Science and Technology Development Agency (NSTDA), Thailand. His research interests include heterogeneous wireless networks, game theory, resource allocations, self-organizing networks, and real time localization systems.



KRIT CHAIWONG received the bachelor's degree in telecommunication engineering from the Mahanakorn University of Technology, Thailand, in 2003, and the M.S. degree from the King Mongkut's Institute of Technology Ladkrabang, Thailand, in 2008, where he is currently pursuing the Ph.D. degree in telecommunication engineering. His current research interest includes telecommunication networks.



LA-OR KOVAVISARUCH (Member, IEEE) received the B.S. degree from the King Mongkut's Institute of Technology Ladkrabang, in 1993, the M.Sc. degree in electrical engineering from Imperial College London, London, U.K., in 1995, and the University of Southern California, in 2001, and the Ph.D. degree in electrical engineering from the University of Missouri-Columbia, in 2005, with sponsorship from the Government of Thailand. From 1993 to 1994, she was a Switching Engineer with TelecomAsia Corporation, Thailand. From 1996 to 1998, she was a Switching Engineer with Siemens Ltd., Thailand, where she was working for a wireless telecommunication client in Thailand. She is currently working as a Researcher with the Department of Telecommunication, National Electronics and Computer Technology Center, Thailand. Her research interests include passive localization and short-range communications.



KAMOL KAEMARUNGS (Senior Member, IEEE) received the bachelor's degree in electronics engineering from the King Mongkut's Institute of Technology Ladkrabang (KMITL), Thailand, in 1994, the M.Sc. degree in interdisciplinary telecommunications program (ITP) from the University of Colorado at Boulder, in 1999, and the Ph.D. degree in information science from the University of Pittsburgh, in 2005. Formerly, he was the Head of the Location and Automatic Identification (LAI) Laboratory, under the National Electronics and Computer Technology Center (NECTEC). He is currently the Research Director of the Communications and Network Research Group (CNWRG) under NECTEC, Thailand. His research interests include ground penetrating radar, ultrawideband sensors, wireless sensor networks, and indoor positioning systems. From 2012 to 2016, he was serving as the Thailand Chapter Chair of the IEEE Communications Society, Asia/Pacific Region 10.



TANEE DEMEECHAI received the B.Eng. degree in electrical engineering from Chulalongkorn University, Bangkok, Thailand, in 1991, and the M.Eng. and D.Eng. degrees from the Asian Institute of Technology, Pathumthani, Thailand, in 1994 and 2000, respectively. In 1995, he was with the Department of Telecommunication Engineering, Mahanakorn University of Technology, Bangkok, as an Assistant Professor. In 2008, he was with Chung-Ang University, Seoul, South Korea, as a Distinguished Visiting Professor, under the support program of IITA. He is currently with the National Electronics and Computer Technology Center (NECTEC), Thailand. His research and technological interests include wireless communications, software-defined radio, and real time localization systems.

...